CHAPTER 3:

Generation of Brillouin Fiber Lasers

In order to explain how we can generate an advanced Brillouin fiber laser (BFL) which is one of the objectives of this thesis, we firstly have to know how BFLs can be generated. Therefore, at the first, we review some experimental results about Brillouin scattering, stimulated Brillouin scattering (SBS) and its threshold, as well as the effects of some factors such as the Brillouin pump (BP)

linewidth and the length of single-mode optical fibers used in this work on the SBS. Then, we pay attention to the generation of BFLs in the ring and Fabry-Perot cavity configurations. Finally, our work will be compared to the earlier work in extracting high efficiency BFLs and multiwavelength BFLs, as an application of BFLs, will be presented at the end of this chapter.

3.1 Observation of Stimulated Brillouin Scattering (SBS)

As mentioned in the last chapter, the frequency of scattered light, known as (BS), is shifted downward due to the Brillouin scattering phenomenon. This can be described classically as an inelastic process in which the incident light is scattered by the acoustical vibrations generated due the electrostriction phenomenon which is the tendency of materials to become compressed in the presence of an electric field. The acoustical vibration can also be interpreted as the moving grating co-propagating with the BP in the forward direction so that the reflected wave has a downshifted frequency due to the Doppler Effect in the backward direction. By using the configuration shown in Fig. 3.1, a BS wave can be obtained readily as demonstrated in Fig. 3.2 by using an Optical Spectrum Analyzer (OSA).

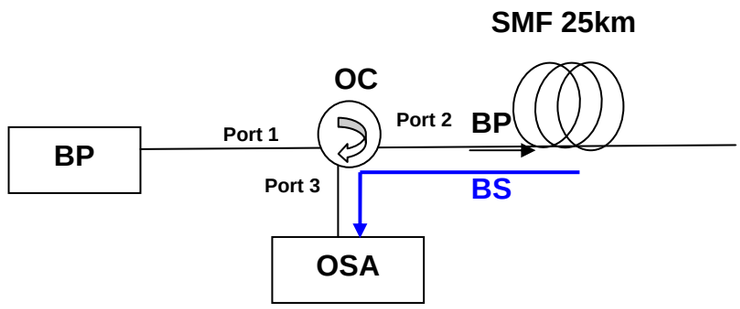

Fig. 3.1: Configuration set-up for Brillouin scattering (BS) detection

Here, we use a Tunable Laser Source (TLS) as the Brillouin pump (BP) with power approximately 5 dBm at the wavelength 1550 nm and the BP wide linewidth 124 MHz. The BP is launched to the 25 km single-mode fiber (SMF) through ports 1 and 2 of the optical circulator (OC) which not only protects the TLS from any reflected light but also provides the output in port 3 for BS power detection using the optical spectrum analyzer (OSA) with a resolution of 0.01 nm. Fig. 3.2 shows the reflection spectrum power from the SMF as it is detected by OSA in the output. The anti-Stokes, the BP Rayleigh reflection and the Brillouin Stokes have powers of about -48.3 dBm, -28.1, and -44.5 dBm, respectively. The BS light wavelength is shifted upward by 0.087 nm from the BP wavelength whereas the anti-Stokes wavelength is downshifted by the same amount but shifted upwards instead due to four-wave mixing. Although we use an optical fiber as the Brillouin cell to observe Brillouin scattering, it can be a gas, a liquid, or any solid with applications in high-power solid-state master oscillator power amplifier (MOPA) systems which provide average output powers up to kilowatt range with diffraction-limited beam quality [1].

BP Reflection

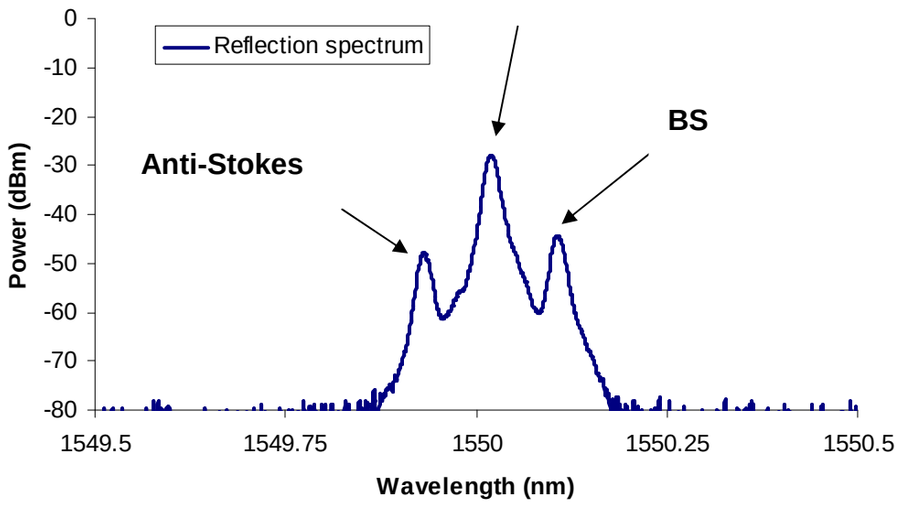

Fig. 3.2: The output spectrum detected by OSA. BP reflection is due to BP Rayleigh scattering whereas the Brillouin Stokes (BS) wave is generated by Brillouin scattering phenomenon. The anti-Stokes wave is due to four-wave mixing between the BP reflection wave and the Stokes wave.

The beat frequency between the scattered BS wave and the incident BP light is equal to the frequency of the acoustic wave. When the interference of the laser pump light and the Brillouin Stokes wave reinforces the acoustic wave, it, in turn, causes the amplification of the scattered Brillouin Stokes wave so that stimulated Brillouin scattering (SBS) happens. In fact, the interaction between the incident wave and the scattered wave in the Brillouin cell can become nonlinear if the interference between the two optical fields can coherently drive an acoustic wave either through electrostriction or through local density fluctuations resulting from the absorption of light and consequent temperature changes. The pump power at which SBS is suddenly increased is called the Brillouin threshold power. Even though the nonlinear Brillouin process is a function of the incident light intensity, in using any gas, liquid or solids, stronger focusing does not decrease the SBS thresholds. The reason for this behavior is the reduced active volume when

stronger focusing is applied. One way to reduce the Brillouin threshold power is the use of waveguide structures which have been used in optical fibers [2],[3],[4] and in capillaries [5] where a high intensity is obtained along the full length of fiber in contrast to the bulk geometry. Nevertheless, if very narrow waveguide diameters are used, damage of the incident surface in addition to volume damage inside the capillary are the limiting factors for the maximum power.

In order to further study the SBS effect, we have to apply a higher BP power to reach the SBS saturation power. Therefore, in this work, an Erbium doped fiber (EDF) amplifier (EDFA) is used to boost the TLS output power. In this case, the combination of the TLS and EDFA is called the Brillouin pump (BP). The EDF used in the experiment has an Er^{+3} ion concentration of 440 ppm, a numerical aperture of 0.21, and a cutoff wavelength 920 nm. The EDF is pumped by a laser diode at the pump wavelength of 980 nm with the maximum output power of 60 mW. As a result, we prepare the BP with the maximum output power about 14 dBm. By changing the BP power, we can see the evolution of the anti-Stokes, the BP reflection, and the Brillouin Stokes. The results are shown in Figure 3.3 in which the increase in the peak power of the anti-Stokes, the BP Rayleigh reflection, and the Brillouin Stokes are demonstrated for various BP powers from 1 dBm to the maximum pump power of 14 dBm. With this 13 dB increase in BP power as shown in Fig. 3.3, , the Brillouin Stokes power is boosted by 45 dB due to the SBS effect whereas the peak power of the anti-Stokes and the BP Rayleigh reflection are increased by only about 7 dB and 12 dB respectively.

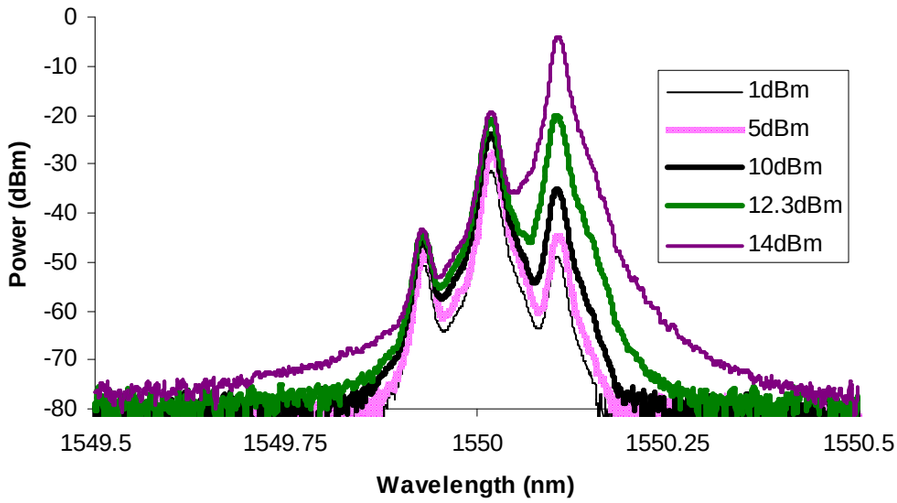

Fig. 3.3: The evolution of anti-Stokes, Rayliegh back scattered BP, and Brillouin Stokes is demonstrated by changing the BP power. Although the peak power of the anti-Stokes and the BP reflection is not changed by much, the Brillouin Stokes peak power is increased a lot due to the SBS effect in increasing BP power from 1 dBm to 14 dBm with the same BP linewidth of 124 MHz.

3.1.1 Effect of BP Linewidth on the SBS

In Eq. (2.103) of the pervious chapter, it is mentioned that the SBS threshold power increases by the factor $[1+(\Delta\nu_{\mathrm{P}}/\Delta\nu_{B})]$ where $\Delta\nu_{\mathrm{p}}$ is the BP bandwidth and $\Delta\upsilon_{\mathrm{B}}$ is the Brillouin gain bandwidth or FWHM of the Brillouin gain curve which is typically of the order of tens of MHz, for example 35 MHz in fused silica with a BP wavelength of 1550 nm [6]. Thus, the Brillouin threshold power is reduced when a narrower BP linewidth is used. Using the narrow BP linewidth 15 MHz, we repeat the procedure leading to Fig. 3.3 and the results are shown in Fig 3.4.

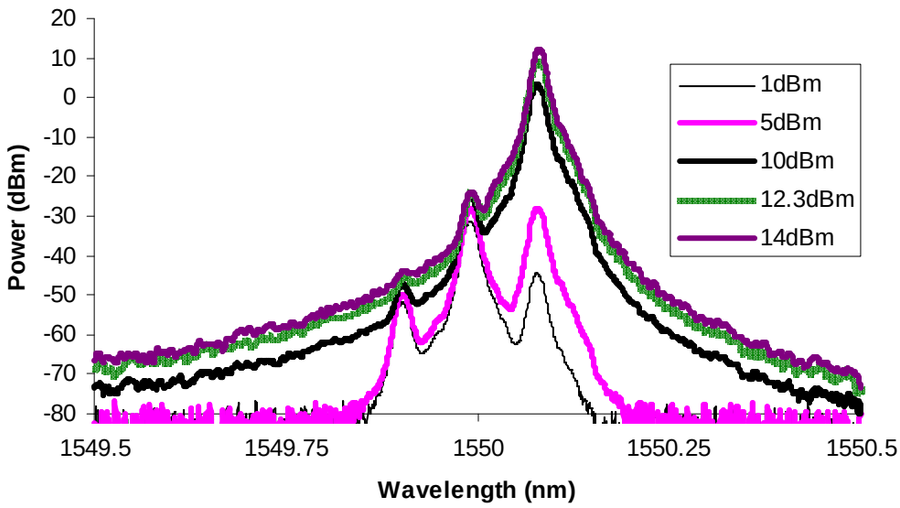

Fig. 3.4: The evolution of anti-Stokes, Brillouin Pump (BP) Rayleigh back scattered BP, and Brillouin Stokes at various BP power obtained by using the narrow linewidth 15MHz.

As shown in Fig. 3.4, the Stokes peak power for BP power 10 dBm and above is much higher compared with the pervious BP power in Fig. 3.3. This is due to the usage of BP narrow linewidth which reduces the SBS threshold power and the Brillouin peak power. With BP linewidth of 15 MHz, the peak power of the anti-Stokes and the BP Rayleigh reflection are increased only about 8 dB and 7 dB respectively, whereas the Brillouin Stokes power is boosted by 57 dB when the BP power is increased from 1 dBm to 14 dBm.

Fig. 3.5 shows the Brillouin Stokes (BS) peak power measured against the BP power at the wide and narrow BP linewidths of about 15 MHz and 124 MHz, respectively. As shown in Fig. 3.5, the narrow linewidth contributes to a higher output power of the BS and a lower BS operation threshold. In the BP power range lower than -2 dBm, the BS peak power for the both BP linewidths of 15 MHz and

124 MHz increase linearly as the BP power increases. However, as the BP power exceeds the critical power value, the BS power rapidly increases. The slope of the graph is approximately measured to be about to 1.21 and 1.24 both before and after the critical power levels for the BP linewidths of 15 MHz and 124 MHz, respectively. Defining the SBS threshold power as the BP power at the critical power level, we can obtain the SBS threshold Power which is at approximately 5 dBm and 12.5 dBm at the BP linewidths of about 15 MHz and 124 MHz respectively, as shown in Fig. 3.5.

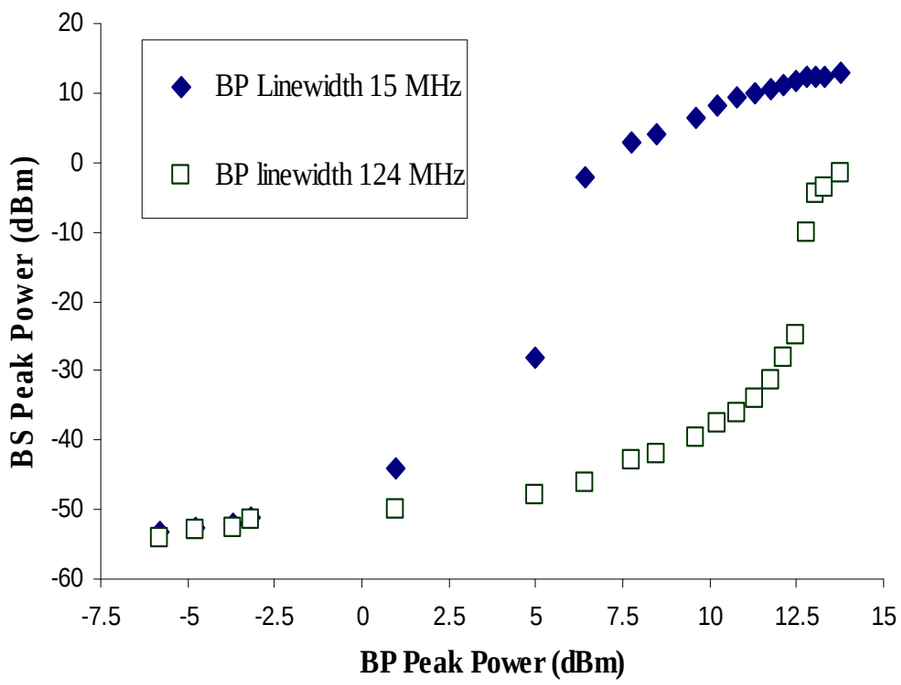

Fig. 3.5: Brillouin Stokes peak power versus BP power in using the different BP linewidths 15 MHz and 124 MHz; see section 4.2. When BP power is above 0 dBm, the BFL peak power increases more in using the BP linewidth 15 MHZ than 124 MHz due to the reduction of the Brillouin threshold power.

3.1.2 Effect of the Fiber Length and Effective area on SBS

The nonlinear interaction depends on the transmission length and the cross-sectional area of the fiber. By using a longer link length, more interactions and a

stronger effect of the SBS will be obtained as a kind of nonlinear phenomena. However, as the signal propagates along the link, its power decreases due to fiber attenuation. Thus, most of the nonlinear effects occur at the input part of the fiber span and diminishes as the signal propagates. The SBS threshold power also decreases by a factor $(1/\mathrm{L}_{\mathrm{eff}})$, in which $\mathrm{L}_{\mathrm{eff}}$ is proportional to the length of the fiber according to Eq. (2.99). In fact, modeling this effect can be quite complicated, but in practice, a simple model assumes that the power is constant over a certain effective length $\mathrm{L}_{\mathrm{eff}}$; this model has proved to be quite sufficient in understanding the effect of nonlinearities such as SBS. Suppose *Po* denotes the power transmitted into the fiber and $P(z) = P_0 \exp(-\alpha z)$ denotes the power at some distance z along the link, where α is the fiber attenuation. If L denotes the actual link length, the effective length (see Fig. 3.6), L_{eff} defined by:

$$P_0 L_{eff} = \int_{z=0}^{z=\mathrm{L}} P(z)dz \tag{3.1}$$

which yields exactly Eq. (2.99). This length $\mathrm{L}_{\mathrm{eff}}$ is chosen in a manner that the area under the curve $P(z) = P_0 \exp(-\alpha z)$ plotted in Fig. 3.6 (a) is equal to the area of the rectangle in 3.6 (b).

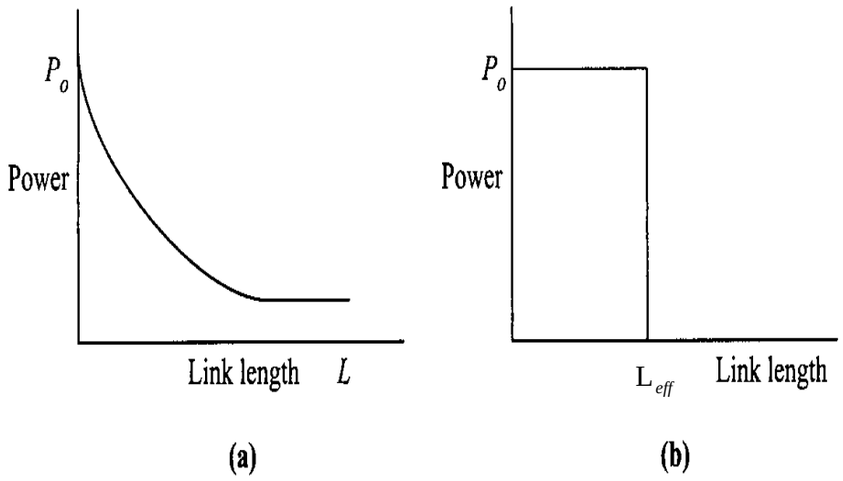

Fig. 3.6: Effective transmission length calculation is depicted. (a) A typical distribution of the power along the length L of a link according to $P(z) = P_0 \exp(-\alpha z)$. The peak power is *Po.* (b) A hypothetical uniform distribution of the power along a link up to define the effective length L_{eff}. This length L_{eff} is chosen in a manner that the area under the curve in (a) is equal to the area of the rectangle in (b).

On the other hand, the SBS threshold saturates when the fiber length is longer than a certain value $(1/\alpha)$ where α, the attenuation constant, is a measure of total fiber loss from all sources. In our case, $\alpha = 0.192$ (dB/km) $= 0.0437$ (km)$^{-1}$ so that $L_{eff} = 22.87$ *km*.

In addition to the fiber length, the effect of nonlinearities also increases with the intensity in the fiber. For a given power, the intensity is inversely proportional to the area of the core as demonstrated by Eq. (2.103) for SBS threshold power. Since the power is not uniformly distributed within the cross section of the fiber. It is convenient in fiber optics literature that one uses an effective cross-sectional area

A_{eff} (see Fig.3.7). The effective area is related to the actual area A and the cross-sectional distribution of the fundamental mode $F(r,\theta)$ by:

$$A_{eff} = \frac{[\int |F(r,\theta)|^2 r dr d\theta]^2}{[\int |F(r,\theta)|^4 r dr d\theta]} \tag{3.2}$$

where (r,θ) denotes polar coordinates. The effective area, as defined above, is a very important parameter which most nonlinear effects such as SBS can be expressed in terms of the effective area for the fundamental mode propagating in the given optical fiber. As shown in Fig. 3.7 (b), the intensity distribution in a fiber is nonzero only for an area A_{eff} around the center of the fiber.

For example, the effective intensity of a propagating laser beam is given by $I_{eff} = \frac{P}{A_{eff}}$, where P is the power of the laser beam, in order to calculate the impact of the nonlinear effect as we will see below. The effective area of SMFs and DSFs is typically about $85\,\mu m^2$ and $50\,\mu m^2$, respectively, whereas for DCFs it is even smaller in order to exhibit higher nonlinearities.

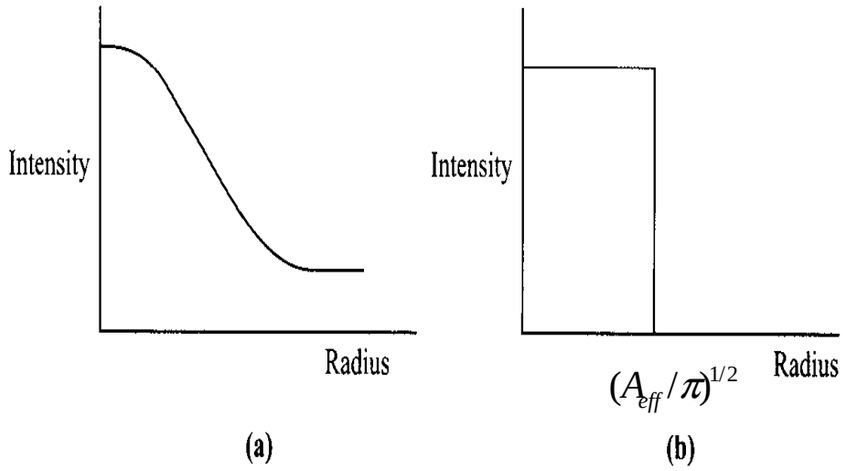

Fig. 3.7: Effective cross-sectional area is depicted against the radius of the fiber. (a) A typical distribution of the signal intensity along the radius of the fiber is demonstrated. (b) A hypothetical intensity distribution of, equivalent to that in (a) for many purposes, shows an intensity distribution that is nonzero only for an area A_{eff} around the center of the fiber.

In this work, by observing the spectra in the same manner that obtained in the Figs. 3.3 and 3.4 and by using different lengths of the optical fiber, the effect of the fiber length on the peak power of the anti-Stokes, BP Rayleigh scattering, and Brillouin Stokes can be investigated. The results are shown in Fig. 3.8 (a) and (b). In this experiment, the BP power is fixed at 14 dBm.

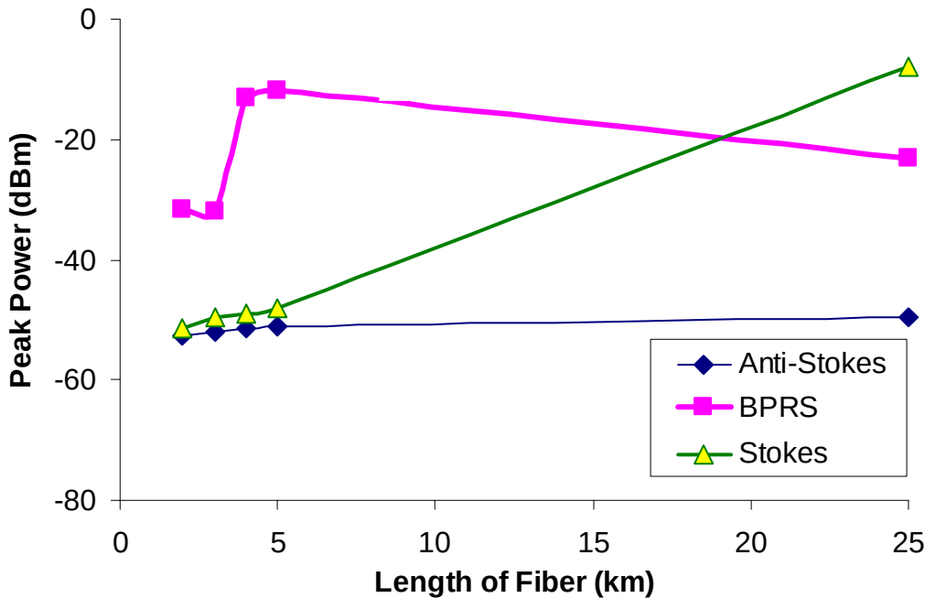

(a)

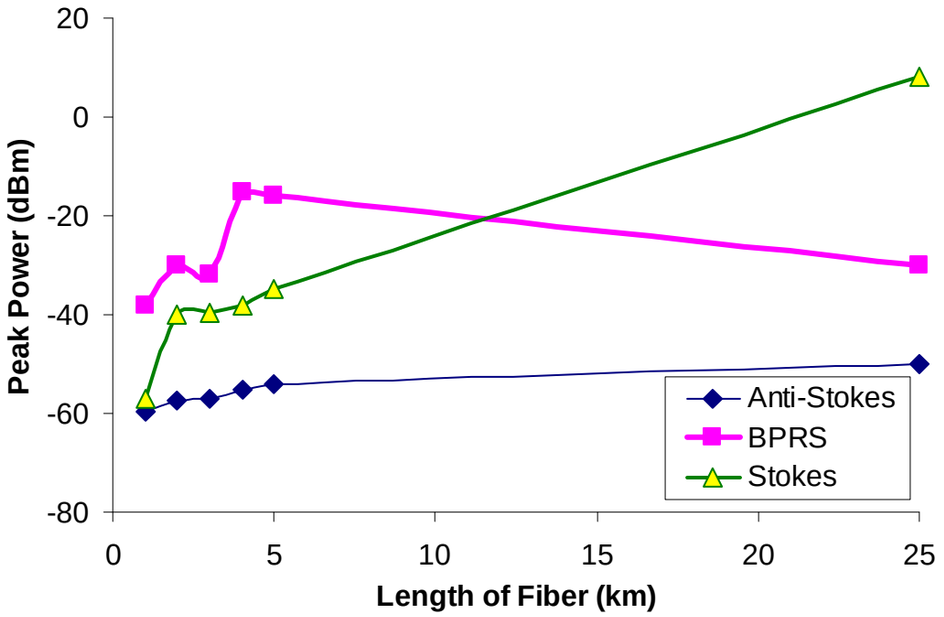

(b)

Fig 3.8: Effect of the fiber length on the peak power of anti-Stokes, Brillouin pump (BP) Rayliegh scattering (BPRS), and Brillouin Stokes. The applied BP peak power is approximately 14 dBm with (a) the wide linewidth 124 MHz and (b) the narrow linewidth 15 MHz. The anti-Stokes peak power is also changed since anti-Stokes is generated by four-wave mixing between Brillouin pump (BP) Rayliegh scattering and Brillouin Stokes waves as mentioned before in Fig. 3.2.

As shown in these figures, the Brillouin Stokes power increases as the length of SMF reaches the effective length L_{eff} due to the increased interaction along the fiber. The used fiber lengths 1 km, 2 km, 3 km, 4 km, 5 km, and 25 km are according to the available fiber lengths in our laboratory. In addition, with the same fiber length, Brillouin Stokes power is higher when narrower BP linewidth is applied due to the dependence of Brillouin threshold power on the BP linewidth which was mentioned before in Eq. (2.103). The reduction of the BP Rayleigh scattering power in the usage of the 25 km fiber length is due to BP depletion occurring during SBS process.

3.1.3 Evaluation Methods of the SBS threshold

In using Eq. (2.103) for determining SBS threshold power, we have to know the Brillouin gain peak $g_B^{(0)}$ which is an intrinsic parameter related to the material. The typical $g_B^{(0)}$ value of fused silica glass is about $g_B^{(0)} = 5\times10^{-11}\,\mathrm{m/W}$ [7]. However, it was reported that the effective $g_B^{(0)}$ value in a single-mode fiber is closely related to the refractive index profile [8]. Hence, exact measurement of the Brillouin gain is needed to evaluate the SBS threshold power in an optical fiber using Eq. (2.103) [9].

In practice, different definitions for estimating the SBS threshold power have been proposed in literatures as the following:

1) The input BP power at which the emerging backscattered power equals the input power [6], [10].

2) The input BP power at which the Stokes power equals the transmitted power [11], [12].
3) The input BP power required to produce the Stokes power at the level of Rayleigh back scattering power [13].
4) The input BP power at which the Stokes power begins to increase rapidly or equivalently, the transmitted BP power begins to be saturated [14], [15].
5) The input power at which the Stokes power at the fiber input is equal to 1% of the input BP power at this point [16], [17].
6) The input power level at which the reflected BP power becomes 4% of the input power [18].

The first definition of SBS threshold power implies BP power at which Stokes power reflected out of the fiber begins to exceed the power launched into the optical fiber. However, it seems impractical since the backscattered power is always less than the input power due to pump depletion. This assumption is based on the idea that the Stokes wave builds up due to the amplification of spontaneous noise in an optical fiber. However, it was shown that definition (1) corresponds to the input BP power at which the Stokes power equals approximately 10% of the input power at the near end of the optical fiber. It was also reported that by choosing the definition (5) for the SBS threshold power, the factor 21 in Eq. (2.102) should be replaced with the number 18 [17]. It is important to note that the definitions (1), (3), (5) and (6) have an advantage over (2) and (4) in which BP saturation or BP depletion is the indicator sign. In fact in the definitions (1), (3), (5) and (6), only two absolute power measurements of the input and the backscattered power are needed rather than three power measurements in methods (2) and (4) where it is also a requirement to indicate the transmitted power.

Fig. 3.9 (a) and (b) show the peak power of the anti-Stokes, BP Rayleigh scattering and Brillouin Stokes against the BP peak power at different BP linewidth of 124 MHz and 15 MHz, respectively. In order to find the SBS threshold in this work, the definition (3) will be used since the three peak power of the anti-Stokes, BP Rayliegh scattering (BPRS) and the Brillouin Stokes can be detected simultaneously. SBS threshold power is evaluated by using the intersection of the BP reflection and the Brillouin Stokes.

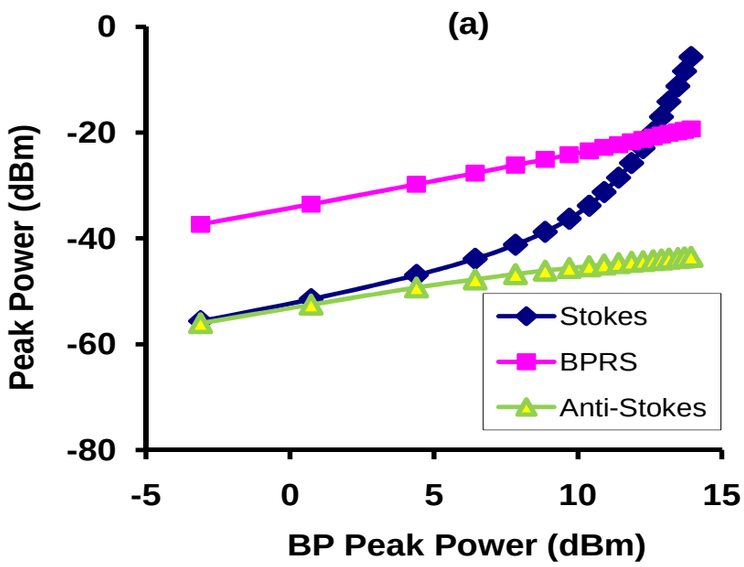

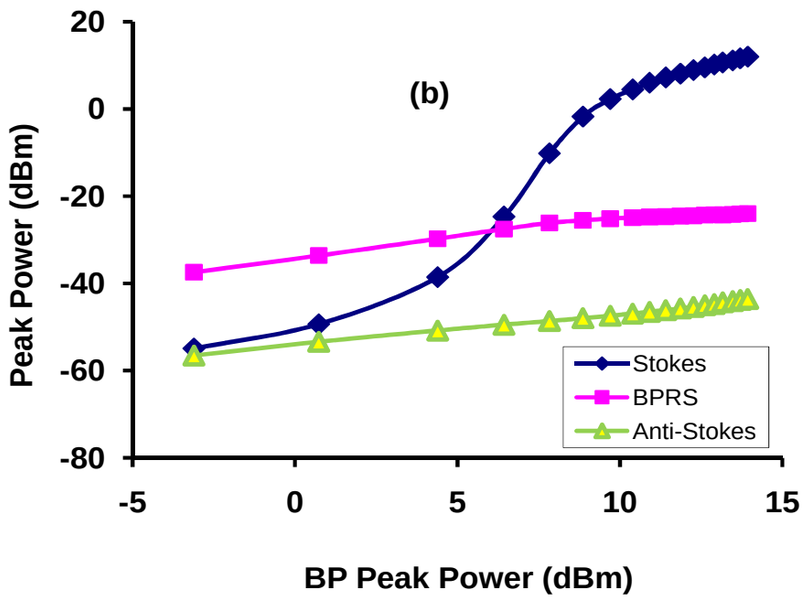

Fig. 3.9: Evaluation of SBS threshold power by using the intersection of BP Rayliegh scattering (BPRS) and Brillouin Stokes for BP linewidth (a) 124 MHz and (b) 15 MHz. The threshold power is the corresponding BP peak power of the intersection point.

Fig. 3.9 (a) and (b), the intersection for wide and narrow BP linewidths are measured to be approximately 12.6 dBm and 6 dBm, respectively. Thus, the Brillouin threshold power for a free end SMF with a length of about 25 km are 12.6 dBm and 6 dBm in using a BP linewidth of 124 MHz and 15 MHz, respectively.

For applications involving SBS, such as Brillouin fiber lasers, Brillouin amplifiers, microwave signal processors, optical sensors, and gyroscopes [19],[20], it is desirable to have a medium that has a large Brillouin gain coefficient g_B given by Eq. (2.81) in order to reduce the SBS threshold power and also the fiber length for the usages in compact devices. Although many crystals and organic materials

are reported to have a large Brillouin gain coefficient [21], many are difficult to draw in the form of optical fibers. So far a number of non-silica based fibers are successfully drawn into optical fibers, which include tellurite, bismuth, and chalcogenide glass fibers. These optical fibers have large nonlinear Kerr and Raman gain coefficients, and thus have potential applications in high-speed optical signal processing [22],[23]. A tellurite fiber with a relatively large refractive index of about 2.028 which is about 40% higher than that of silica [24], is expected to exhibit a large Brillouin scattering coefficient since it is proportional to the material refractive index raised to the power of about 7 (n^7) [25]. Chalcogenide fiber is also reported to have a Brillouin gain coefficient about two orders of magnitude larger than of silica-based fibers [26].

In addition, it is also known that the SBS threshold can be decreased using feedback. Different loop schemes providing the feedback for bulk SBS materials were investigated [27]. In these methods, part of the Brillouin Stokes' light is fed back into the SBS material. Using this feedback, a self-seeding of the SBS process takes place; thus the SBS Stokes' signal increases. At the same time, a part of undepleted residual Brillouin pump light is also fed back into the SBS cell. The injection of the undepleted Brillouin pump also decreases the SBS threshold further due to the intensifying of the injected BP. This is an important issue because fibers, due to the existence of high intensities in their small core have already reduced the SBS threshold by many orders of magnitude compared to the bulk material. Nevertheless, a further SBS threshold reduction which is possible by using a feedback scheme would be of interest especially for continuous wave (CW) and quasi-CW lasers with medium average power in the range of several tens of Watts. It was also shown that even Fresnel reflection at the fiber end

surface can decrease the SBS threshold; however, a chaotic behavior of the reflected Brillouin Stokes' light results by using very long fibers in the feedback mechanism [28]. In the following section, the various kinds of feedback mechanism will be discussed.

3.2 Generation of Brillouin Fiber Lasers

In this section, the feedback schemes in the form of ring cavities and linear cavities will be demonstrated to generate Brillouin Stokes' oscillation which, in turn, causes Brillouin fiber lasers (BFLs) generation. Typical linear and ring cavities which are used for generating linear and ring BFLs are shown in Fig. 3.10 (a) and (b) respectively. In the linear cavity, the linear laser is assumed to have two counter-propagating BFL beams at the laser wavelength whereas in ring cavities, only one unidirectional BFL beam can propagate in the opposite direction with respect to the BP direction due to the Brillouin scattering feature in optical fibers.

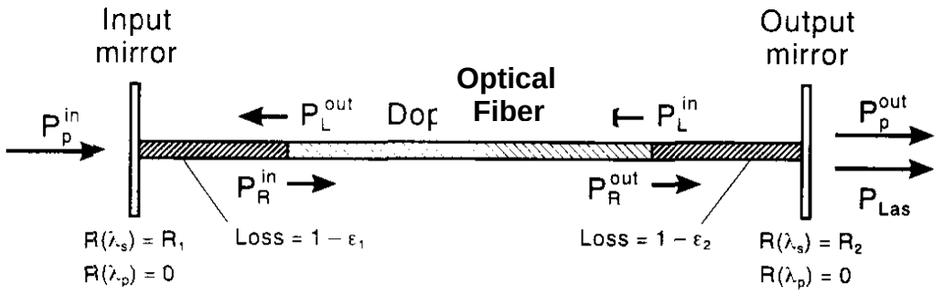

(a)

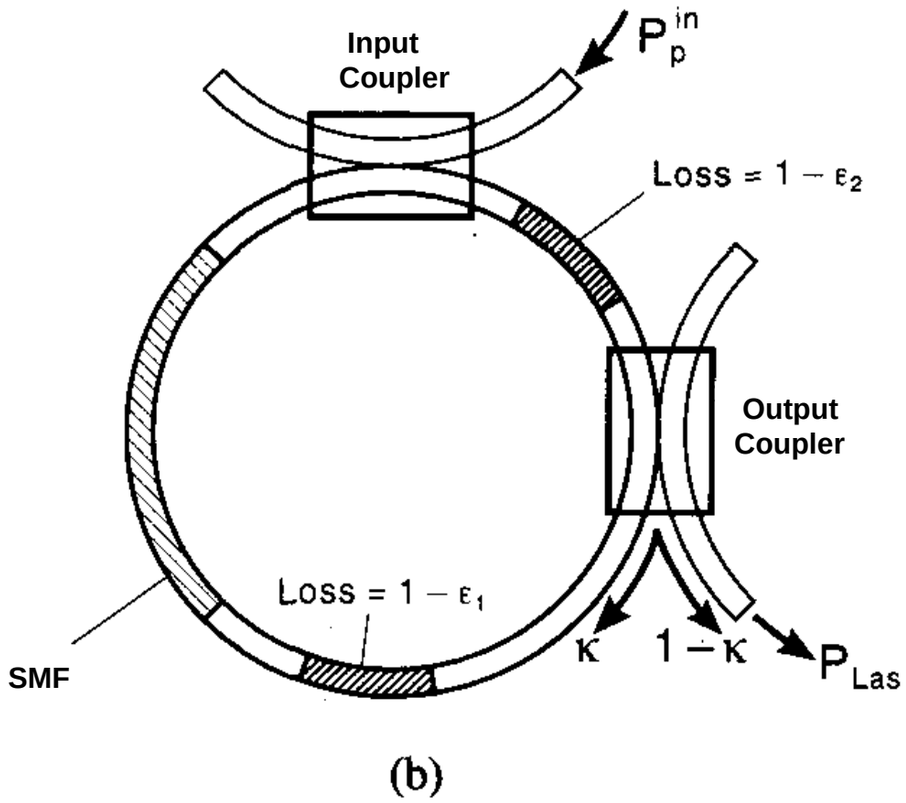

Fig. 3.10: Brillouin Fiber laser configurations for (a) linear laser and (b) ring laser.

For the linear laser shown in Fig. 3.10 (a), the left-hand side mirror has reflectivity R_1, and the right-hand side mirror has reflectivity R_2, at the lasing wavelength. Both mirrors are transparent at the pump wavelength so that the pump has only one pass through the fiber. P_p^{in} is the pump light that inputs to the optical fiber. Single-pass transmissions of ε_1 and ε_2 account for intracavity components such as tuning elements and the fiber-to-mirror coupling loss for each discrete loss elements. At any point in the fiber, there is pump light propagating to the right and a laser light standing wave that is a superposition of right- and left-propagating laser lights.

The output laser power P_{Las} is given by

$$P_{Las} = (1 - R_2)\varepsilon_2 P_R^{out} \tag{3.3}$$

where P_R^{out} is the power at the fiber-laser wavelength out from the right hand side end of the optical fiber.

The nonlinear dynamics of Brillouin fiber lasers plays an important role in fiber optics. Under the one-dimensional approximation which is customary in single-mode fibers (SMFs), SBS is fairly well understood in the frame of the coherent 3-wave model of SBS [29], [30], as mentioned before in Eqs. (2.104) and (2.105). This model accounts for perturbative optical Kerr effect and spontaneous noise [31]. Brillouin fiber laser (BFL) devices exhibit periodic, quasi-periodic [32-35], chaotic [36], and even solitonic super- and sub-luminous pulse propagation [37], [38], as well as self-stabilization of the phase which yields ultra-coherent regimes leading to BFL linewidths as narrow as a few hertz [39],[40]. Due to the very high Brillouin gain in a long enough single-mode fiber which allows very low finesse and reinjection rates, BFLs are fairly simple to operate with only tens of mW of Brillouin pump. According to the modal analysis [41], the linear laser and the ring laser globally exhibit the same dynamics. Depending on the fiber length, three distinct dynamical behaviors can be distinguished:

(i) For fiber lengths lower than a critical value L_c which is 48 m in ring cavities and 11m in ring cavities, the SBS emission remains stable for any input pump power. This can be interpreted within the framework of a modal analysis. In this case, the cavity free spectral range (FSR) is comparable with the width of the Brillouin gain curve, and only a few modes can experience gain. Near the threshold, only the mode that coincides with the center of the gain curve has sufficient gain to overcome the resonator losses and can oscillate. Since the

Brillouin curve is homogeneously broadened, the laser always remains monomode as the input power increases [42].

(ii) For long enough fibers, the SBS emission is unstable just beyond the threshold. In this case, the resonator FSR is so small that many of the modes close to the center of the gain curve nearly experience the same gain and can oscillate simultaneously near the threshold. This leads to the unstable behaviors observed in previous works [43-48].

(iii) The transition between the dynamical behaviors observed in the two previous cases (short and long fibers) occurs inside a range of intermediate lengths. The SBS emission, stable and therefore monomode near the threshold, becomes unstable for sufficiently high pumping levels.

Note that, for any fiber length, the "Brillouin mirror" regime may be reached by sufficiently increasing the pumping level. The modal analysis, previously introduced in order to describe the laser's behavior near the threshold, also allows us to explain the difference between the values of the critical lengths obtained for the ring laser (48 m) and for the Fabry-Perot laser (11 m). For a given fiber length, the Fabry-Perot FSR is half that of the ring cavity. Thus, if the two resonators had the same quality factor, the critical length characterizing the Fabry-Perot would be half that of the ring laser (i.e., 24 m). However, in the numerical simulations used in the modal analysis [41], the Fabry-Perot quality factor is much lower than that of the ring cavity so that the strong overlapping between modes then favors their competition and the critical length is reduced (< 24 m).

The next section discusses generation of BFL in a ring cavity in which we propose a new ring-cavity configuration which can result in higher BFL power in comparison to the traditional one [49]. Then in the following section, the linear cavity BFL will be discussed in which the generation of the enhanced BFL will be

explained by proposing a new linear cavity configuration in fiber optics [50]. Finally we pay attention to our work in the linear cavity BFL generation in which two Bragg gratings are used instead of the mirrors [51].

3.2.1 Brillouin Fiber Lasers with Ring Cavities

Stimulated Brillouin scattering in a continuous wave-pumped low-finesse fiber ring resonator is called Brillouin fiber ring laser (BFRL) when the closed-loop gain exceeds unity so that Brillouin amplification overcompensates the ring cavity loss. Thus, a cavity length of several meters is required to obtain threshold power in the milliwatt range by preparing the SBS nonlinear gain. The bandwidth of the Brillouin gain is very narrow, typically from 20 to 50 MHz for the wavelength in the near infrared region, but its magnitude is fairly small [52]. But long cavities result in narrow resonance in the frequency domain and sub-Megahertz linewidth of cavity modes as soon as the cavity length exceeds a few meters and sub-Megahertz linewidth of cavity modes is observed as soon as the cavity length exceed a few meter. Therefore, BFLs are generally constructed in an all-fiber, high-finesse ring-resonator arrangement to achieve low laser threshold and efficient operation [53]. BRFLs have attracted considerable interest because of their varied type of dynamic behavior [54-59].One of the most important features of BFRLs is the existence of periodic intensity modulation in the created Brillouin Stokes signal. This effect, called self-pulsing has been studied in detail [54].

When studies of BRFLS were first formulated, no information about the instability of SBS was given since the transient effect of the acoustic wave and optical Kerr effect inducing self- and cross-phase modulations were neglected in this model [60]. A more realistic formulation of the fiber ring laser was then given by the coherent three-wave model, considered in obtaining Eqs. (2.104) and

(2.105), [46], [61] where the acoustic damping was taken into account, and then a Hopf bifurcation between steady and pulsed regimes was evident [55]. It is also known that SBS instabilities including periodic, quasi-periodic and chaotic oscillations may arise only when the length of the fiber cavity is large enough [54], [56]. The experimental results also show that the Brillouin emission is stable for a short fiber at any input power [56]. Therefore, the physical origin of the instabilities in a BFRL is attributed to the existence of a large number of longitudinal modes beneath the Brillouin gain curve rather than to the optical Kerr effect [54], [58]. Moreover, it is generally considered that the SBS instability, especially the self-pulsing phenomenon may be suppressed by the use of a short and high-finesse cavity [58]. In such a cavity, the threshold of SBS would be greatly reduced [62], [63] and the transient Stokes intensity in the ring could significantly exceed the steady-state value [60].

In most of the previous papers about the SBS effect in a fiber ring resonator, both the pump and Stokes waves have been assumed to be resonant within the cavity. The linear phase detuning of the cavity for either the circulating pump wave or Stoke wave has not been considered. However, it should be noted that this assumption is very rough and even incorrect when the finesse of the cavity is high enough. In fact, the difference between the total linear phase ϕ_p (accumulated by the pump wave) and ϕ_s (accumulated by the Stokes wave) per round trip of the cavity is much larger than the magnitude 2π even if the length of the fiber resonator is several centimeters. In a high-finesse ring resonator, since the circulating pump power depends strongly on the linear phase detuning of the cavity, the difference between ϕ_p and ϕ_s must be considered in the theoretical calculation.

Fig 3.11 shows two configurations of the ring BFL. In optical fibers, since the frequency shift of the Brillouin Stokes vanishes in the forward direction which is the direction of the Brillouin pump (BP) propagation, according to Eq. (2.58), Brillouin Stokes propagates only in the backward direction in respect to BP. In this study, a new BFL ring cavity configuration is proposed using components similar to the conventional BFL, but the new BFL has a higher output power as compared to the conventional BFL. The experimental setup for the conventional BFL configuration is shown in Fig. 3.11 (a) in which a 3-dB coupler and a 25 km single-mode fiber (SMF) act as a ring resonator. The anti-clockwise propagating BFL is routed to the Optical Spectrum Analyzer (OSA) via the 3 port optical circulator. Fig. 3.11 (b) shows the new configuration, which uses components similar to the conventional configuration. In this configuration the resonator consists of an optical circulator, the coupler and the SMF. However, here, the coupler is placed between the SMF and port 3 of the optical coupler extracts only the counterclockwise output BFRL power detected by the OSA. The SMF which is spliced between ports 2 and 3 of the optical circulator through the coupler to generate the BFL ring resonator. The SMF is 25 km in length and has a cut-off wavelength of 1161 nm with a zero dispersion wavelength of 1315 nm and a mode field diameter of 9.36 µm. Both BFRLs are pumped by an external cavity tunable laser source (TLS) as the Brillouin pump (BP) with a maximum power of approximately 5.5 dBm in the narrow linewidth setting. Due to the maximum BP power limitation and the Brillouin threshold reduction, the trend of BFRLs can be studied better by using the narrow BP linewidth 15 MHz. In the Fig. 3.11(b), the Brillouin pump (BP) with the 15 MHz linewidth is injected into the SMF from port 1 through port 2 of the optical circulator in a clockwise direction. The backward-propagating SBS generated oscillates inside the resonator in anti-clockwise

direction to generate the Brillouin laser, which is coupled out using a 3 dB coupler. The optical circulator which protects the TLS from any BP reflection is also used to force the unidirectional operation of the laser in the cavity although SBS in the SMF propagates only in the backward direction due to the SBS feature. The laser output is characterized using an Optical Spectrum Analyzer (OSA) with a resolution of 0.015 nm.

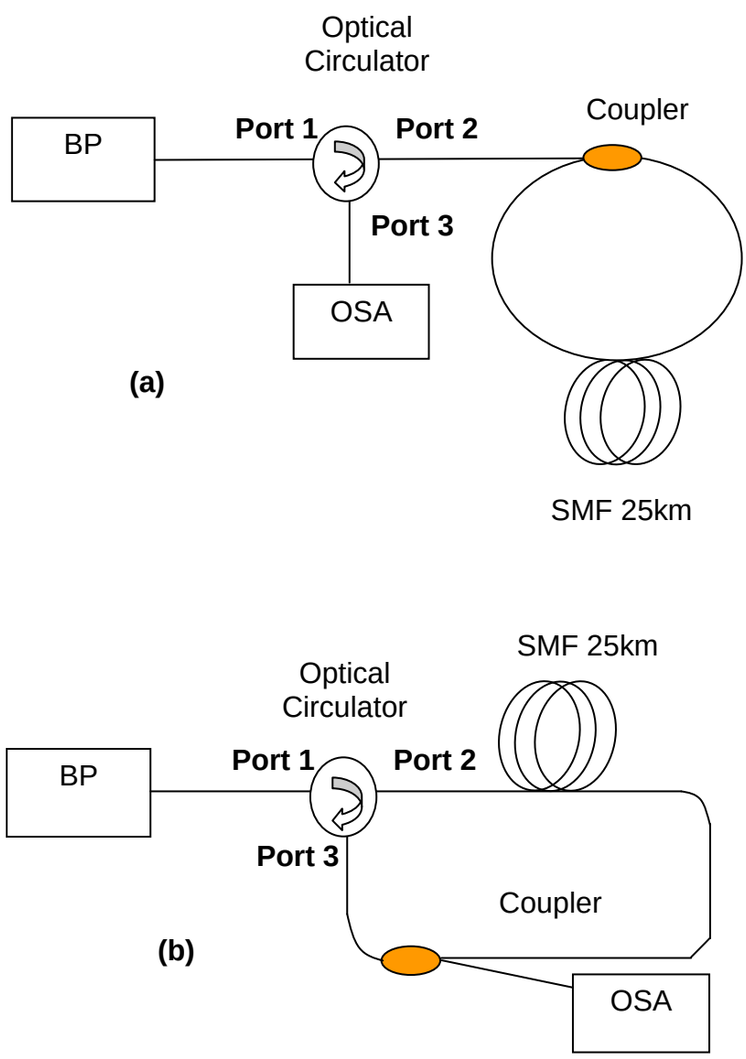

Fig. 3.11: Experimental set up for the generation of (a) a conventional BFRL and (b) the proposed new configuration BFRL.

The results are shown in Fig. 3.12 which compares the output spectrum for the conventional BFRL and the proposed new BFRL configuration. The 3-dB coupler (50-50) allows half of the light to oscillate in the cavity and another half to couple out as the output of the BFRL. Both BFRL configurations generate a Brillouin laser at around 1550.1 nm, which is 0.08 nm longer than the BP wavelength. The anti-Stokes signal is also observed at a shorter wavelength due to four-wave mixing between the BP wave and the Brillouin Stokes wave. The proposed BFRL configuration of Fig. 3.11(b) shows an output peak power of -0.5 dBm, which is 5.7 dB higher compared to the conventional configuration in Fig. 3.11(a). The anti-Stokes signal also shows a 1.8 dB increment in signal power. Even though the cavity loss is smaller in the conventional configuration due to using only the SMF and the coupler in the ring resonator, the proposed configuration is configured such that the SMF receives more BP power. In other words, the higher BP power generates higher back-propagating Brillouin Stokes power and the Brillouin gain in the cavity. Therefore the BFL and the SBS anti-Stokes powers are higher in the proposed BFL configuration as compared to the conventional BFL configuration. The Brillouin crosstalk effect also causes the anti-Stokes and BP Rayleigh reflection power to be transferred to the BFRL power.

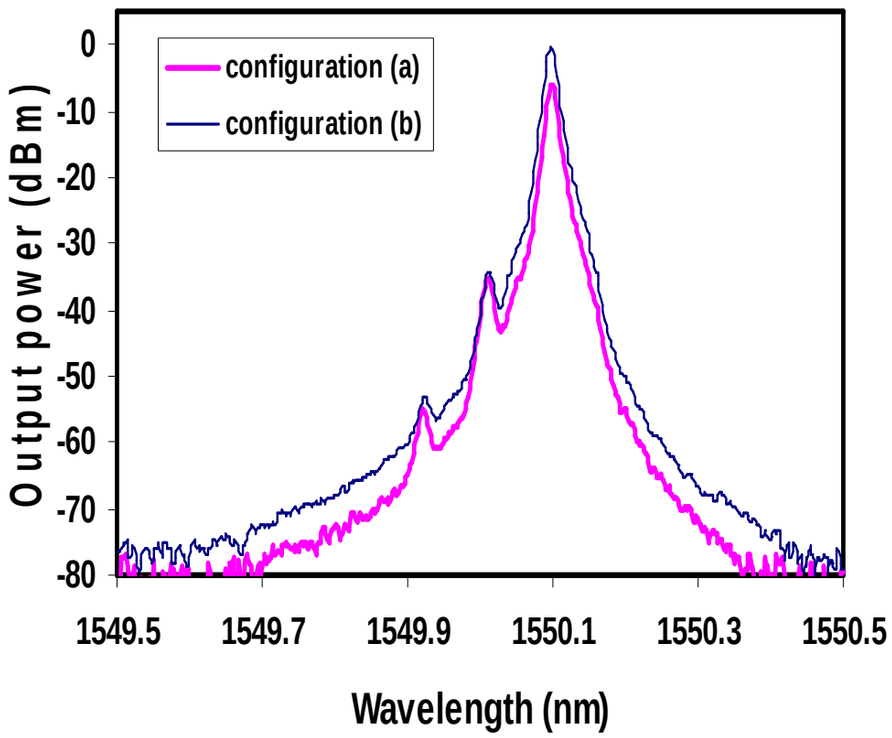

Fig. 3.12: The Comparison of the BFRL output spectrum between the conventional configuration (a) and the proposed configuration (b) shown in Fig 3.11.

Fig. 3.13 shows the BFL output spectrum of the proposed new configuration of Fig. 3.12(b) at the different output coupler ratios. The BP power is fixed at 5.5 dBm and the length of SMF is 25 km in all the measurements. The line spacing is approximately 0.08 nm in the wavelength domain and 11GHz in the frequency domain, as measured by an optical spectrum analyzer with a resolution of 0.015 nm. The 3-dB bandwidth of each BFRL line is less than 0.02nm, limited by the OSA resolution. However, the bandwidth measurement will be done by using the heterodyne method which will be explained in the next chapter. As shown in Fig. 3.13, the laser peak power is increased by decreasing the output leg power ratio

due to the increasing BP power which reaches the SMF. However, the output BFRL peak power decreases as the output leg power ratio decreases by 20%. This is attributed to the saturation of the Brillouin Stokes power and the small amount of light being extracted out of the cavity by reducing the coupler ratio. The maximum output power was observed at 0.5 dBm with an output coupler of 20-80 ratio, where 80% of the light is allowed to oscillate in the cavity and 20% of the light is coupled out as output, as shown in Fig. 3.13 [49].

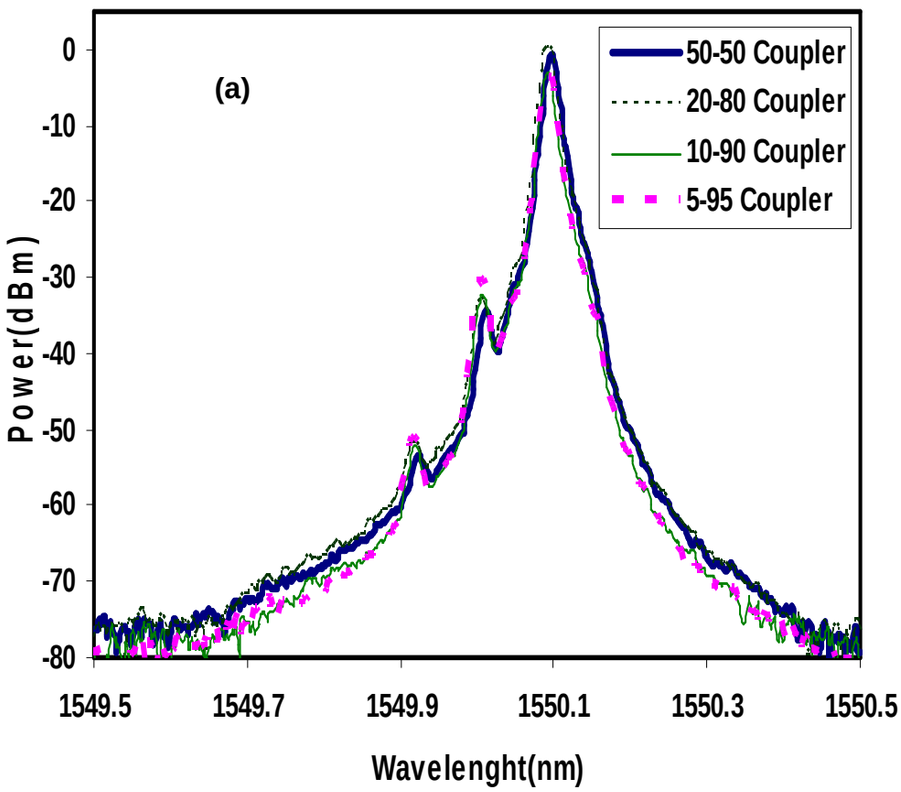

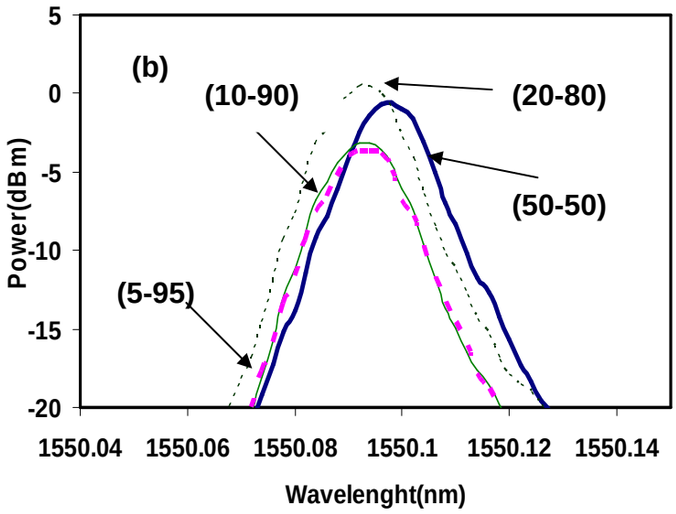

Fig. 3.13: (a) The BFRL output comb at different output coupler ratios. (b) The enlarged figure of the output peak region is shown for the comparison. The slight shift in the BFL wavelength is due to the small BP wavelength shift which is in turn the result of the environment condition variation effect on TLS.

3.2.2 Generation of Brillouin Fiber Lasers in Linear Cavities

Previous BFLs have been set up using ring cavities and a few BFLs, so far, have been presented using a linear configuration. This is due to the fact that conventional-linear-cavity BFLs suffer from some problems such as the generation of higher-order Stokes and anti-Stokes waves. In the following, we will discuss the linear cavities and propose some linear configurations in order to solve the problems.

In a linear cavity, additional feedback from the boundaries is known to give rise to periodic temporal structures in the experiment [64], [65]. In this paper, we demonstrate a new BFL design with a linear cavity. A stable BFL was obtained at a wavelength of 0.08 nm from the pump wavelength 1550 nm through the careful optimization of the output coupling ratio and the employment of a suitable

reflector. The performance of the BFL is done by using different reflectors such as optical circulators and FBGs.

The experimental setup is shown in Fig. 3.14 whereby the linear cavity is formed by two optical circulators in configuration (a), a circulator and a fiber Bragg grating (FBG) in configuration (b) and only a FBG in configuration (c). Here, the SMF characteristics are as the one used before in BFRL generation. The SMF is pumped by the Brillouin pump (BP) which is an external cavity tunable laser source (TLS) amplified by an Erbium-Doped Fiber Amplifier (EDFA). The maximum power of the amplified BP is approximately 14.5 dBm and the BP is injected into the SMF via a 3-dB coupler in the forward direction. The generated backward-propagating SBS oscillates inside the resonator to generate the BFL, which is coupled out via the coupler and the output laser is characterized using an OSA with a resolution of 0.015 nm. The experiment is carried out using three different couplers ratios; 50/50, 95/5 and 99/1. For each coupler, the port of the lower ratio is connected to the TLS and the OSA.

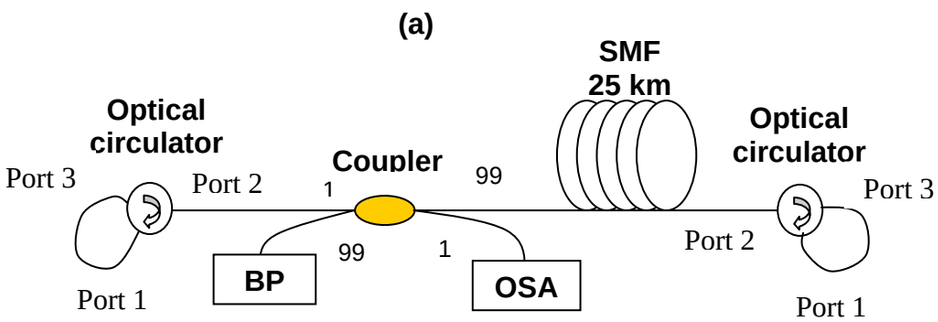

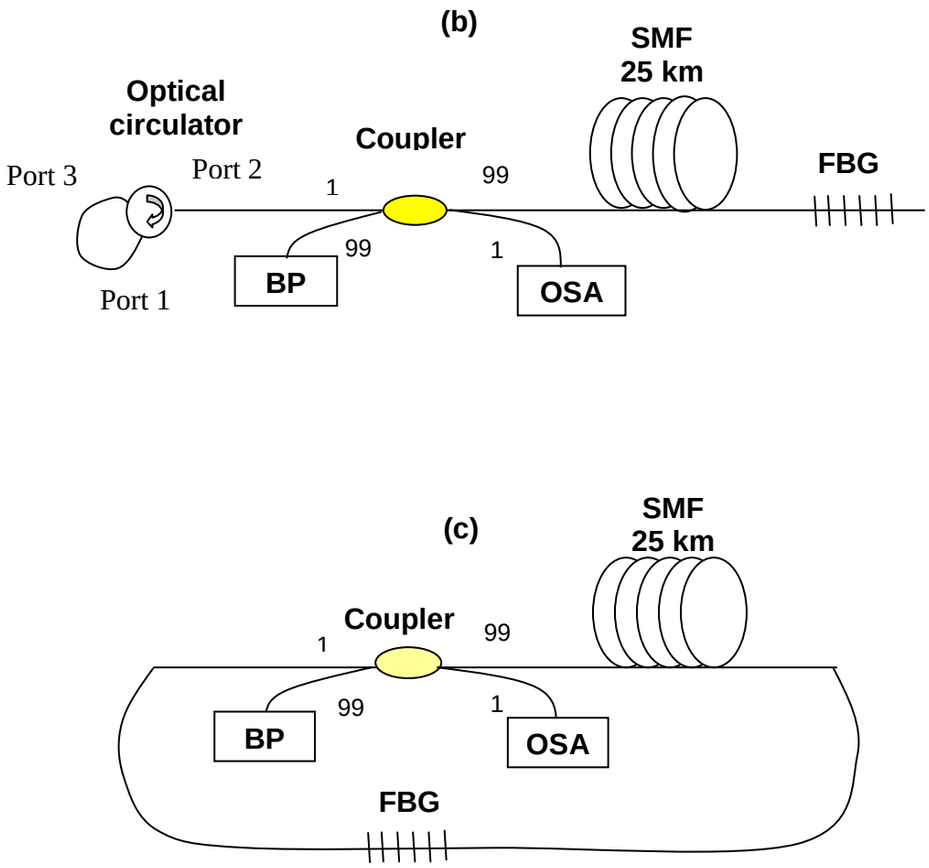

Fig. 3.14: Experimental set up for generating linear cavity Brillouin fiber lasers by using (a) two optical circulators, (b) a circulator and a fiber Bragg grating (FBG), and (c) a FBG.

Fig. 3.15 shows the output spectra of the linear-cavity BFL for each of the mentioned configurations. In this experiment, the coupler ratio was 1/99 and the BP power fixed at 14.5 dBm. The coupler ratio was 1/99 is the best ratio for BFL generation which is discussed in Fig. 3.16. As shown in Fig. 3.15, two simultaneous lines are obtained with the BP line at approximately 1550.011 nm and the BFL line at approximately 1550.094 nm. The laser is generated by the

Brillouin gain which was provided by the 25 km SMF. As the BP is coupled into the SMF, the Brillouin Stokes signal is generated at a frequency shifted by approximately 0.083 nm due to the Brillouin scattering effect. The Stokes propagates in the opposite direction of the BP and travels to the circulator, acting here as a reflector, before it is rerouted back into the SMF by the circulator. The amplified Stokes then travels back to the other side of reflector and this oscillation continues to generate the BFL. The use of an FBG instead of an optical circulator in configurations B and C increases the output power of the laser as shown in Fig. 3.15. The highest output power is obtained with the use of only one FBG as in the configuration C. The BFL peak power is about 0.73 dB higher than that obtained in the configuration B. This is attributed to the reduced loss in the cavity due to the FBG. The FBG used in the experiment has a reflectivity of more than 99.5% at a wavelength region from 1525 to 1560nm. This contributed to a loss of less than 0.1 dB as compared to the circulator loss which is approximately 1 dB. The maximum laser peak power is obtained at -4.5 dBm.

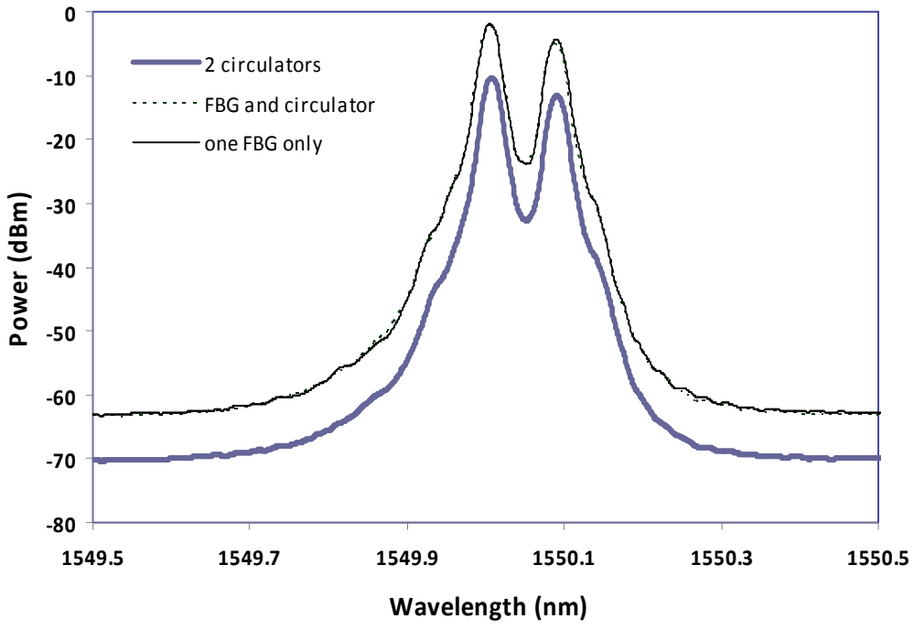

Fig. 3.15: The BFL output spectrum for the different linear cavity configurations at an input BP power of 14.5 dBm**.** The BFL peak power in using one FBG is about 0.73 dB higher than that obtained by using one FBG and an optical circulator.

In Fig. 3.16, the BFL output spectrum is demonstrated by using different coupler ratios in the configuration (a) in Fig. 3.14 with the BP power of 14.5 dBm. If the total Brillouin gain is equal to or higher than the cavity loss, BFL laser oscillation can be formed between the two optical circulators. As shown in Fig. 3.16, the BFL is generated with both 95/5 and 99/1 couplers, which contributes to a lower cavity loss. However, the laser cannot be generated with a 50/50 coupler due to the high loss in the cavity. The highest peak is obtained with a 99/1 coupler which has the lowest cavity loss.

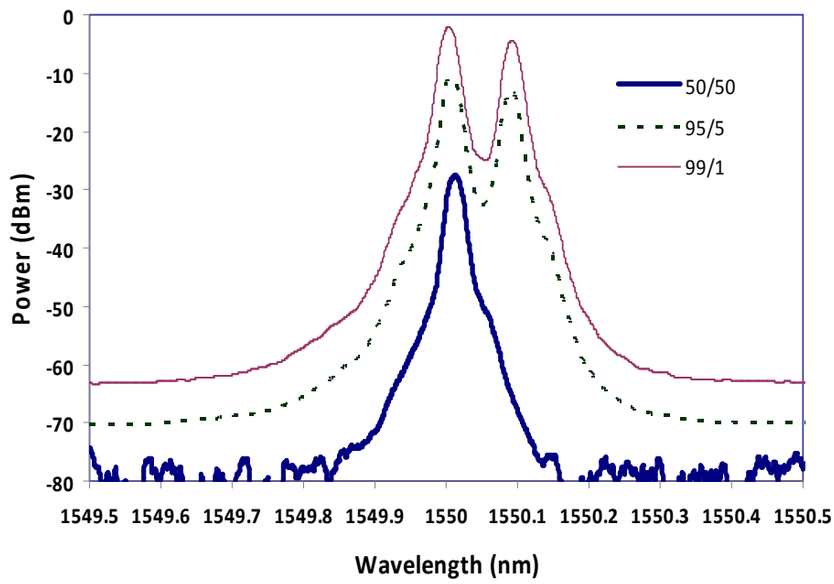

Fig. 3.16: The BFL output spectrum for different coupler ratios used in a linear cavity configuration (a) shown in Fig. 3.14 with the BP power of 14.5 dBm.

The proposed linear configurations demonstrate new linear-cavity designs for the BFL generation. Stable BFL operation was obtained at an up-shifted wavelength of about 0.08 nm from the pump wavelength through the careful optimization of the output coupling ratio and employment of a suitable reflector. An efficient and low cost linear cavity Brillouin fiber laser (BFL) is demonstrated using only a single fiber Bragg grating (FBG) as a reflector. The laser peak is obtained at -4.5 dBm with a Brillouin pump of 14.4 dBm. The use of a 99/1 optical coupler shows the highest output due to the low loss in the cavity [51]. However, the BFL peak power is much less than the transmitted BP power as shown in Figs. 3.15 and 3.16. Some research has been done to solve this problem in order to improve the efficiency in the BFL generation. In this research, a new design for

linear cavities is demonstrated in which the BFL peak power can be higher than the transmitted output BP peak power. Stable operation of the BFL is obtained at an up-shifted wavelength of about 0.086 nm from the pump wavelength.

The proposed configuration is shown in Fig. 3.17 whereby the linear cavity is formed by two optical circulators (OC1 and OC2), a 3-dB coupler and a 95/5 coupler located between ports 3 and 1 of OC1 and OC2, respectively. As before, a 25 km long SMF is used as a gain medium with an attenuation coefficient of 0.19 dB/km at 1550 nm. The BP is injected into the SMF via the 3-dB coupler and OC1 in a forward (clockwise) direction at $z = 0$ as indicated in Fig. 3.17.

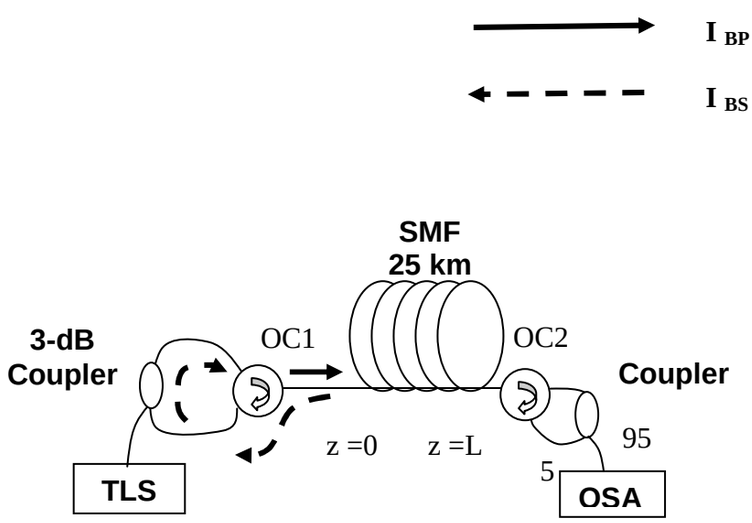

Fig. 3.17: Experimental setup for the proposed linear cavity.

The BP is injected into the SMF via the 3-dB coupler and OC1 in a forward (clockwise) direction at $z = 0$ as indicated in Fig. 3.17. The first backward-propagating Stokes, initiated at $z = L$ from spontaneous Brillouin scattering or seed signal, oscillates inside the resonator to subsequently generate the BFL and the second-order forward-propagating Brillouin stokes which is starts at $z = 0$ through cascaded SBS coupled out via the 95/5 coupler. This coupler also suppresses higher-order anti-Stokes and Stokes generation. The first anti-Stokes arises due to four-wave mixing (FWM) between the co-propagating BP and BFL photons. The output laser is characterized using an OSA with a resolution of 0.015 nm.

Fig. 3.18 compares the output BFL spectrum of the proposed configuration and the conventional configurations. The spectrum of the conventional configuration is that one shown in Fig. 3.16 for the coupler ratio 95/5. As shown in Fig. 3.18, for the proposed configuration, two Stokes lines at approximately 1550.101 nm and 1550.187 nm, and one anti-Stokes at approximately 1549.929 nm are obtained around the oscillated BP at approximately 1550.015 nm whereas we have only the first Stokes in the conventional cavity. However, the first Stokes peak power in the proposed configuration is about 12.3 dB higher than that one resulting in the use the conventional scheme. Also, the Brillouin Stokes peak power is higher than the BP transmitted BP peak power which is a new occcurence encountered in this field [50].

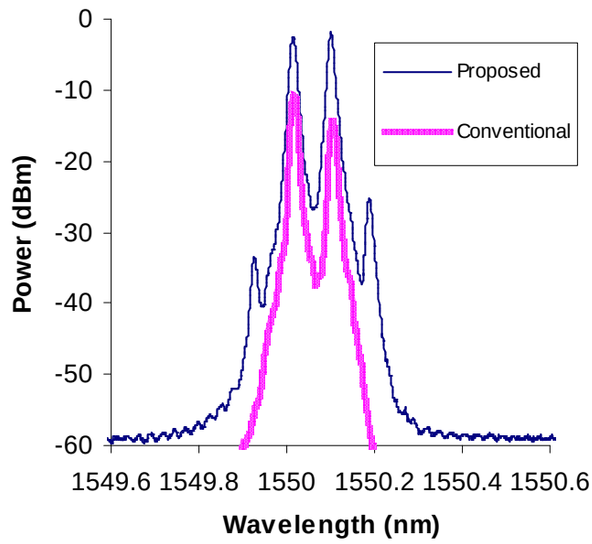

Fig. 3.18: The output spectra for the proposed and conventional configurations at a BP power of 14.4 dBm. The BFL peak power is generated higher than the BP peak power by using the proposed cavity.

As a summary, a new BFRL with higher output power and some linear cavity BFLs are proposed. The last linear cavity BFL configuration has been demonstrated by incorporating a 3-dB coupler, a 95/5 coupler, two optical circulators, and a 25 km SMF that allows very high conversation efficiency compared with the last work [66]. Stable BFL operation was obtained at an up-shifted wavelength of 0.086 nm from the pump wavelength with the BFL peak power at -1 dBm, which is 12.3 dB higher than the conventional BFL with the same BP power 13 dBm, due to the reduced cavity loss in the proposed configuration.

References

[1] R. St. Pierre, D. W. Mordaut, H. Injeyan, J. G. Bery, R. C. Hilyard, M. E. Weber, M. G. Wickham, G. M. Harpole, R. Senn, “Diode array pumped kilowatt laser,”IEEE J. Sel. Topics Quant. Electron. QE-3, pp. 53-58, 1997.

[2] E. A. Kuzin, M. P. Petrov, B. E. Davydenko, “Phase conjugation in an optical fibre,” Opt. Quant. Electron. QE-17, pp. 393-397, 1985.

[3] H. J. Eichler, J. Kunde, B. Liu, “Quartz fibre phase conjugators with high fidelity and reflectivity,” Opt. Commun. vol. 139, pp. 327-334, 1997.

[4] R. G. Harrison, V. I. Kovalev, W. Lu, D. Yu, “SBS self-phase conjugation of CW Nd:YAG laser radiation in an optical fibre,”Opt. Commun. vol. 163, pp. 208-211, 1999.

[5] D. C. Jones, M. S. Mangir, D. A. Rockwell, “A stimulated Brillouin scattering phase-conjugate mirror having a peak-power threshold < 100 W ,”Opt. Commun. vol. 123, pp. 175-181, 1995.

[6] R. G. Smith, “Optical power handling capacity of low loss optical fibers as determined by stimulated Raman and Brillouin scattering,” Applied Opt. vol.11, pp. 2489-2494, 1972.

[7] G. P. Agrawal, *Nonlinear Fiber Optics*, 3rd ed., Academic Press, New York, 2001, chap. 9.

[8] A. B. Ruffin, M. –J. Li, X. Chen, A. Kobyakov, F. Annunziata, “Brillouin gain analysis for fibers with different refractive induces,” Opt. Lett. vol. 30, pp. 3123-3125, 2005.

[9] M. Nikles, L. Thevenaz, P. A. Robert, “Brillouin gain spectrum characterization in single-mode optical fibers,” IEEE J. Lightwave Technol. vol. 15, pp. 1842-1851, 1997.

[10] K. Shiraki et al., “SBS threshold of a fiber with a Brillouin frequency shift distribution,” J. Lightwave Technol. vol.14, pp.55-57, 1996.

[11] W. B. Gardner, “Appendix on Nonlinearities for G. 650”,ITU Document COM 15-273-E, 1996.

[12] T. C. E. Jones, “The validity of single mode optical fiber transfer standard for the calibration of fibers for high power uses,” NPL Report COEM 10, 1998.

[13] X. P. Mao, R. W. Tkach, A. R. Chraplyvy, R. M. Jopson, and R. M. Derosier, “Stimulated Brillouin threshold dependence on fiber type and uniformity,” IEEE Photon. Technol. Lett. vol. 4, pp. 66-68, 1992.

[14] X. P. Mao, R. W. Tkach, A. R. Chraplyvy, R. M. Jopson, and R. M. Derosier, “Stimulated Brillouin threshold dependence on fiber type and uniformity,” IEEE Proceeding of the Optical Fiber Communications Conference, Tech. Dig. OFC/IOOC‘91, San Diego USA, TuK4, pp. 41, 1991.

[15] D. Cotter, “Observation of stimulated Brillouin scattering in low-loss silica fiber at 1.3-μm,”Electron. Lett vol.18, pp. 495-496, 1982.

[16] R. D. Esman et al, “ Brillouin scattering: beyond threshold,” IEEE Proceeding of the Optical Fiber Communications Conference, pp. 227-228, 1996.

[17] P. Bayvel and P. M. Radmore, “Solutions of the SBS equations in single mode optical fibers and implications for fiber transmission system,” Electron. Lett. vol. 26, pp. 434-436, 1990.

[18] T. Shimizu, K. Nakajima, K. Shiraki, K. Ieda, I. Sankawa, “Evaluation methods and requirments for the stimulated Brillouin scattering thresholdin a single-mode fiber,” Opt. Fiber Technol. vol. 14, pp. 10-15, 2008.

[19] S. Norcia, S. Tonda-Goldstein, D. Dolfi, and J. –P. Huignard, “Efficient single-mode Brillouin fiber laser for low-noise optical carrier reduction of microwave signals,” Opt. Lett. vol. 28, pp. 1888-1890, 2003.

[20] F. Zarinetchi, S.P. Smith, and S. Ezekiel, “Stimulated Brillouin fiber optic laser gyroscope,” Opt. Lett., vol.16, pp. 229-231, 1991.

[21] H. Yoshida, M. Nakatsuka, H. Fujita, T. Sasaki, and K. Yoshida, “High-engery operation of a stimulated Brillouin scattering mirror in an L-Arginine phosphate monohydrate crystal,” Appl. Opt. vol. 36, pp. 7738- 7787, 1997.

[22] J. H. Lee, T. Tanemura, T. Nagashima, T. Hasegawa, S. Ohara, N. Sugimoto, and K. Kikuchi, “Use of 1-m Bi_2O_3 nonlinear fiber for 160-Gbit/s optical-time division demultiplexing based on polarization rotation and wavelength shift induced by cross-phase modulation,” Opt. Lett. vol. 30, pp. 1267-1269, 2005.

[23] M. Asobe, T. Kanamori, and K. I. Kubodera, “Applications of highly nonlinear chalcogenide glass fiber in ultrafast all-optical switches,” IEEE J. Quantum Electron. vol. 29, pp. 2325-2333, 1993.

[24] G. Ghosh, “Sellmeier coefficients and chromatic dispersions for some tellurite glasses,” J. Am. Ceramic. Soc. vol. 78, pp. 2828-2830, 1995.

[25] D. Cotter, “Observation of stimulated Brillouin scattering in low-los silica fiber at 1.3 μm,” Electron. Lett. vol. 18, pp. 495-496, 1982.

[26] K. S. Abedin, “Observation of strong stimulated Brillouin scattering in single-mode As_2Se_3 chalcogenide fiber,” Opt. Express vol. 13, pp. 10266-10271, 2005.

[27] G. K. N. Wong, M. J. Damzen, “Investigations of Optical Feedback Used to Enhance Stimulated Scattering,” IEEE J. Quant. Electron. QE-26, pp. 139-148, 1990.

[28] M. Dämmig, G. Zinner, F. Mitschke, H. Welling, “Stimulated Brillouin scattering in fibers with and without external feedback,” Phys. Rev. A vol. 48, pp. 3301-3309, 1993.

[29] J. Botineau, C. Leycuras, C. Montes, E. Picholle,“Stabilization of a stimulated Brillouin fiber ring laser by strong pump modulation,” J. Opt. Soc. Am. B vol. 6, pp.300-312,1989.

[30] C. Montes, D. Bahloul, I. Bongrand, J. Botineau, G. Cheval, A. Mahmoud, E. Picholle, A. Piccozi, “Self-pulsing and dynamic bistability in cw-pumped Brillouin fiber ring lasers,” J. Opt. Soc. Am. B vol. 16, pp. 932-951,1999.

[31] R. W. Boyd, K. Rzazewski, P. Narum, “Noise Initiation of Stimulated Brillouin Scattering, “Phys. Rev. A vol. 42, pp. 5514-5521, 1990.

[32] I. Bar-Joseph, A. A. Friesem, E. Lichtman, R. G. Waarts, “Steady and relaxation oscillations of stimulated Brillouin scattering in single-mode optical fibers ,” J. Opt. Soc. Am. B vol. 2, pp. 1606-1611, 1985.

[33] A. L. Gaeta, R. W. Boyd, “Stimulated Brillouin scattering in the presence of feedback ,”Int. J. Nonlinear Opt. Phys. vol. 1, pp. 581-594, 1992.

[34] C. Montes, A. Mamhoud, E. Picholle, “Bifurcation in a cw-pumped Brillouin fiber-ring laser: Coherent soliton morphogenesis,” Phys. Rev. A vol. 49, pp. 1344-1349, 1994.

[35] S. Randoux, V. Lecoeuche, B. Segard, J. Zemmouri, “Dynamical analysis of Brillouin fiber lasers: An experimental approach,” Phys. Rev. A vol. 51, R4345 - R4348, 1995.

[36] D. Yu, W. Lu, R. G. Harrison, “Observation and characterization of deterministic chaos in stimulated Brillouin scattering with weak feedback ,”Phys. Rev. A vol. 49, R24-R27, 1994.

[37] E. Picholle, C. Montes, C. Leycuras, O. Legrand, J. Botineau, “Observation of dissipative superluminous solitons in a Brillouin fiber ring laser,” Phys. Rev. Lett. vol. 66, pp. 1454-1457, 1991.

[38] C. Montes, A. Picozzi, D. Bahloul, “Dissipative three-wave structures in stimulated backscattering. II. Superluminous and subluminous solitons,” Phys. Rev. E vol. 55, pp. 1092-1105, 1997.

[39] S. P. Smith, F. Zarinetchi, S. E. Ezekiel, “Narrow-linewidth stimulated Brillouin fiber laser and applications,” Opt. Lett. vol. 16, pp. 393-395, 1991.

[40] M. Nikles, L. Thevenaz, Ph. A. Robert, “Brillouin gain spectrum characterization in single-mode optical fibers,” IEEE J. Lightwave Technol. vol. 15, pp. 1812- 1851, 1997.

[41] S. Randoux, V. Lecoeuche, B. Segard, and J. Zemmouri, “Dynamical analysis of Brillouin fiber lasers: An experimental approach,” Phys. Rev. A vol. 51, pp. 4345-4348, 1995.

[42] O. Svelto, *Principle of Lasers*, 3 rd Ed. New York, Plenum Press, 1989.

[43] M. Dämming G. Zinner, F. Mitschke, and H. Welling, “Stimulated Brillouin scattering in fibers with and without external feedback,” Phys. Rev. A vol. 48, pp. 3301-3308, 1993.

[44] R. G. Harrison, P. M. Ripley, and W. Lu, “Observation and characterization of deterministic chaos in stimulated Brillouin scattering with weak feedback,” Phys. Rev. A vol. 49, pp. R24-R27, 1994.

[45] E. Picholle, C. Montes, C. Leycuras, O. Legrand, and J. Botineau, “Observation of dissipative superluminous solitons in a Brillouin fiber ring laser,” Phys. Rev. Lett. vol. 66, pp. 1454-1457, 1991.

[46] J. Botineau, C. Leycuras, C. Montes, and E. Picholle, “Stabilization of a stimulated Brillouin fiber ring laser by strong pump modulation,” J. Opt. Soc. Am. B, pp. 300-312, 1989.

[47] I. Bar-Joseph, A. A. Friesem, E. Lichtman, and R. G. Waarts, “Steady and relaxation oscillations of stimulated Brillouin scattering in single-mode optical fibers,” J. Opt. Soc. Am. B vol. 2, pp. 1606-1611,1985.

[48] C. Montes, A. Mamhoud, and E. Picholle, “Bifurcation in a cw-pumped Brillouin fiber-ring laser: Coherent soliton morphogenesis,” Phys. Rev. A vol. 49, pp. 1344-1349, 1994.

[49] M. R. Shirazi, S. W. Harun, K. Thambiratnam, M. Biglary, H. Ahmad, “New Brillouin fiber laser configuration with high output power,” Microwave and Optical Technology Letters vol. 49, pp.2656-2658, 2007.

[50] M. R. Shirazi, S. W. Harun, M. Biglary, and H. Ahmad, “Linear cavity Brillouin fiber laser with improved,” Opt. Lett. vol. 33, pp. 770-772, 2008.

[51] H. Ahmad, M. R. Shirazi, M. Biglary, S. W. Harun, “Linear cavity Brillouin fiber laser using a fiber Bragg grating,” Microwave and Optical Technology Letters vol. 50, pp. 265-266, 2008.

[52] N. Nikles, L. Thevenaz, and P. A. Robert, “Brillouin gain spectrum characterization in single-mode optical fibers,” J, Lightwave Technol. vol. 15, pp. 1842-1851, 1997.

[53] S. P. Smith, F. Zarinetchi, and S. Ezekiel, “Narrow-linewidth stimulated Brillouin fiber laserand applications,” Opt. Lett. vol. 16, pp. 393-395, 1991.

[54] C. Montes, D. Bahloul, I. Bongrand, J. Botineau, G. Cheval, A. Mamhoud, E. Picholle, and A. Picozzi, “Self-pulsing and dynamic bistability in cw-pumped Brillouin fiber ring lasers,”J. Opt. Soc. Am. B vol.16, pp. 932-951, 1999.

[55] C. Montes, A. Mamhoud, E. Picholle, “Bifurcation in a cw-pumped Brillouin fiber-ring laser: Coherent soliton morphogenesis,” Phys. Rev. A. vol. 49, pp. 1344-1349, 1994.

[56] S. Randoux, V. Lecoeuche, B. Segard and J. Zemmouri, “Dynamical analysis of Brillouin fiber lasers: An experimental approach,” Phys Rev A vol. 51, pp. R4345-4348, 1995.

[57] S. Randoux, V. Lecoeuche, B. Segard and J. Zemmouri, “Dynamical behavior of a Brillouin fiber ring laser emitting two Stokes components ,” Phys Rev A vol. 52, pp. 2327-2334,1995.

[58] V. Lecoeuche, B. Segard, and J. Zemmouri, “Modes of destabilization of Brillouin fiber ring lasers,’Opt. Commun. vol. 134, pp. 547- 558, 1997.

[59] E. Picholle and A. Piccozi,“Guided-acoustic-wave resonances in the dynamics of a stimulated Brillouin fiber ring laser,” Opt. Commun. vol. 135, pp. 327- 330, 1997.

[60] P. Bayvel, I. P. Giles and P. M. Radmore, “Transient and steady-state characteristics of a Brillouin amplifier based on an all-fiber single-mode ring resonator,” Opt. Quantum Electron,” Opt. Quantum Electron. vol. 21, pp. S113-S128 ,1989.

[61] J. Bontineau, C. Leycuras, C. Montes, “CW-pumped polarization-maintaining Brillouin fiber ring laser: I. Self-structuration of Brillouin Solitons,” and “CW-pumped polarization-maintaining Brillouin fiber ring laser: II. Active mode-locking by phase modulation,” Opt. Commun. vol. 257, pp. 319-333, 2006.

[62] L. F. Stokes, M. Chodorow, and H. J. Shaw, “All-fiber stimulated Brillouin ring laser with submilliwatt pump threshold,” Opt. Lett. vol. 7, pp. 509-511, 1982.

[63] R. Kadiwar and I. P. Giles, “Effects of stimulated Brillouin scattering on the performance of polarization-maintaining all-fiber ring resonators,”Opt. Lett. vol. 14, pp. 332-334, 1989.

[64] R. V. Johnson, and J. H. Marburger, “Relaxation Oscillations in Stimulated Ruman and Brillouin Scattering,” Phys. Rev. A vol. 4, pp. 1175-1182,1971.

[65] I. Bar-Joseph, A. A. Friesem, E. Lichtman, and R. G. Waarts, “Steady and relaxation oscillations of stimulated Brillouin scattering in single-mode optical fibers,” J. Opt. Soc. Am. B vol. 2, pp. 1606-1611, 1985.

[66] V. Lecoeuche, P. Niay, M. Douay, P. Bernage, S. Randoux and J. Zemmouri, “ Bragg grating based Brillouin fiber laser,” Optics Commun. vol. 177, 303-306, (2000).